On the Nuclear Rotation Curve of M31

Thomas S. Statler
Department of Physics and Astronomy, 251B Clippinger Research Laboratories, Ohio University, Athens, OH 45701, USA

ABSTRACT

The nuclear rotation curve of M31, as observed by the *Hubble Space Telescope* Faint Object Camera Spectrograph, shows a significant disturbance coinciding with the off-center brightness peak, P1. This $\pm 60\,\mathrm{km\,s^{-1}}$ feature is distinguished by a local velocity maximum centered on P1 and a local minimum $\sim 0\farcs08$ closer to P2. If the M31 double nucleus is an eccentric disk with an off-center density concentration, as suggested by Tremaine, then the self-gravity of the disk can produce just such a disturbance. The expected kinematic signature is calculated approximately by examining sequences of closed periodic orbits in a Kepler potential perturbed by a model disk potential that precesses at constant frequency. The perturbation forces a steep negative eccentricity gradient in the sequence of closed orbits through the densest part of the disk, which reverses the arrangement of periapsis and apoapsis with respect to the central mass. Stars making up the inner part of the density concentration are at apoapsis, while stars making up the outer part are at periapsis, producing a steep local velocity gradient. This result is independent of the details of the mass distribution. The projected rotation curve of the model is shown to closely resemble that of M31, giving strong support to the eccentric disk picture.

Subject headings: galaxies: individual (M31)—galaxies: kinematics and dynamics—galaxies: nuclei

1. Introduction

Currently viable explanations for the double-peaked structure of the nucleus of M31 revealed by the *Hubble Space Telescope* (*HST*; Lauer et al. 1993, 1998) center around two basic scenarios: first, that the off-center brightness peak, P1, represents a transient structure, possibly a star cluster on the verge of tidal disruption (Emsellem & Combes 1997); second, that P1 is an equilibrium configuration, resulting from a statistical accumulation of stars near the apoapsides of their orbits in an eccentric ring or disk (Tremaine 1995, hereafter T95). Groundbased spectroscopy at arcsecond (Bacon et al. 1994) and better (Kormendy & Bender 1999, hereafter KB99) resolution shows asymmetries in the rotation and dispersion profiles across the two brightness peaks. These asymmetries are in the sense expected in the eccentric disk picture, prompting KB99 to argue in strong support

of the T95 model. However, the sinking-cluster scenario has enough adjustable parameters that, with sufficient perseverance, an adequate fit to the data could probably be found.

The highest resolution kinematic data to date come from the f/48 long-slit spectrograph of the *HST* Faint Object Camera (FOC; Statler et al. 1999, hereafter SKCJ). The FOC rotation curve is completely consistent with the groundbased data, when the former is convolved to the resolution of the latter. In addition, the FOC data show kinematic features at smaller scales. The most significant is a disturbance to the rotation curve in P1, superficially resembling a barely resolved local rotation in the same sense as the overall rotation of the nucleus (fig. 4c below). The FOC data are limited by low signal-to-noise (S/N) ratio, and confirmation by upcoming Space Telescope Imaging Spectrograph (STIS) observations is certainly desirable. However, the "P1 wiggle" is found in the region of highest S/N in the FOC data, and the peak-to-peak amplitude of $\sim 120\,\mathrm{km\,s^{-1}}$ is robust and insensitive to details of the reduction process.

It is difficult to argue that the P1 wiggle could be a natural consequence of the sinking cluster scenario. If P1 is a bound object, its luminosity ($\sim 10^6\,L_\odot$) and characteristic radius ($\sim 1\,\mathrm{pc}$) would suggest a severely tidally truncated, collapsed-core globular cluster. But a rotation velocity $\sim 60\,\mathrm{km\,s^{-1}}$ would correspond to $V/\sigma > 1$, at least two times higher than observed in Galactic globulars (e.g., Gebhardt et al. 1997) or inferred from the their flattenings (Davoust & Prugniel 1990). Spin-up by an earlier tidal interaction with the central black hole (BH) is conceivable, but it is hard to see how such an interaction could have avoided disrupting the cluster.

On the other hand, a local distortion to the rotation curve of this magnitude may be a natural consequence of the eccentric disk picture. The shape of the distortion suggests that the self-gravity of the disk may be at work. It is easy to see how such a feature could arise in the simple case of a massive *circular* ring centered on the BH. The ring pulls outward on objects in its interior; thus the ring potential would lower the circular velocity for orbits just inside the ring, and raise it for orbits just outside, distorting the rotation curve in the sense observed. Of course, this distortion would be seen symmetrically on both sides of the center. In this *Letter*, I show that the self-gravity of an eccentric disk will naturally produce the same kind of feature in the rotation curve—though for a different reason—only on one side, as is seen in the FOC data.

The plan of this *Letter* is as follows: In § 2 I construct a simple model for a non-self-gravitating eccentric disk, whose parameters are consistent with the T95 model for M31. The purpose of the initial model is only to provide a plausible density distribution, from which I calculate a plausible perturbation to the otherwise Keplerian potential. In § 3, I examine the closed periodic orbits in the perturbed potential, in a frame rotating at an assumed precession speed Ω_p; these orbits will be the parents of more general quasi-periodic orbits that will be populated in the self-gravitating disk. The character of the perturbation forces a steep negative eccentricity gradient in the sequence of orbits moving outward through the densest part of the disk. This gradient reverses the arrangement of periapsis and apoapsis, such that stars making up the inner part of the density concentration are at apoapsis, while stars making up the outer part are at periapsis. Elementary considerations

of celestial mechanics show why this must be the case, independent of the details of the mass distribution. While self-consistent models are outside the scope of this *Letter*, I estimate in § 4 the effect on the rotation curve by integrating the closed-orbit velocity field over an aperture approximating the FOC slit and show that the expected signature is qualitatively close to the observed rotation curve. Finally, I discuss in § 5 the implications for more realistic models and the prospects for using details of the rotation curve to constrain the masses of the disk and BH.

2. Mass Distribution in an Eccentric Disk

To calculate a plausible density distribution, I assume a cold, infinitesimally thin disk of stars on aligned elliptical Kepler orbits. I place the BH of mass M at the origin and the common line of apsides along the x axis in a cartesian system, with periapsides at positive values of x. The eccentricity e as a function of semimajor axis a in the initial model is specified by a fixed function $e(a)$, which I assume changes sufficiently slowly that the orbits are not mutually intersecting. The gravity of the bulge is ignored.

For a mass dM distributed in a phase-independent way around a single orbit, the mass per unit length ℓ would be given by dM/vP, where v is the instantaneous speed and P the period. For a continuum of orbits labeled by their semimajor axes a and populated so that the mass per unit interval of a is $\mu(a)$, the mass in the area $da\,d\ell$ at (a,ℓ) is $dM = \mu(a)da\,d\ell/vP$. Replacing a by length s measured perpendicular to the orbit introduces a factor $da/ds = |\nabla a|$. Writing this factor explicitly in terms of the eccentricity law $e(a)$, and using the standard formulae for Kepler orbits, I obtain for the surface density of the disk, after some algebra,

$$\Sigma(a,x) = \frac{\mu(a)}{2\pi a}\frac{(1-e^2)^{1/2}}{1-e^2-(2ae+x)e'}. \tag{1}$$

In equation (1), x is the cartesian coordinate and $e' \equiv de/da$. Note that having a density maximum at apoapsis ($x = -a[1+e]$) requires that the eccentricity decrease outwards.

A particularly simple choice for $e(a)$ that is qualitatively consistent with the behavior in the T95 model is

$$e(a) = \frac{\Delta}{a}. \tag{2}$$

Equation (2) implies that the orbits are all confocal, sharing the focus at the origin occupied by the BH and the empty focus at $x = -2\Delta$. The surface density of a confocal disk takes on a simple form in the elliptic coordinate system (u,w) defined by

$$x = \Delta(\cosh u \sin w - 1), \qquad y = \Delta \sinh u \cos w. \tag{3}$$

In these coordinates each orbit follows an ellipse $u =$ constant, and the surface density is given by

$$\Sigma(u,w) = \frac{\mu(\Delta\cosh u)}{2\pi\Delta\cosh u}\frac{\tanh u}{\cosh u + \sin w}. \tag{4}$$

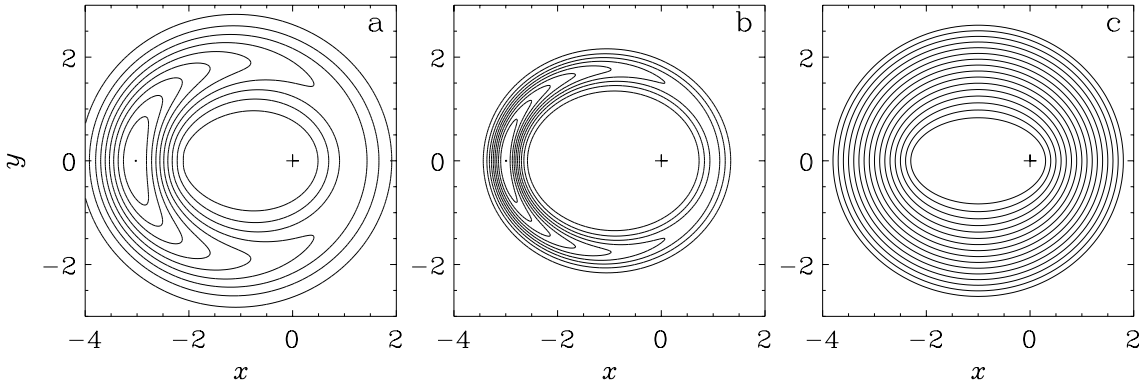

Fig. 1.— (a) Density contours for a "wide" eccentric disk built from confocal, aligned Kepler orbits, with the mass distribution as given in eq. (6) and width $\sigma = 0.5$. Contours are at $0.1, 0.2, \ldots, 1.0$ of the maximum density. Cross marks the central point mass. (b) Same as (a), but for the "narrow" disk, with $\sigma = 0.2$. (c) Representative orbits in the disks, following the eccentricity law in eq. (2).

The potential can be computed by standard methods, most efficiently by an expansion in suitable basis functions. For this work I simply evaluate the integral

$$\Phi = -\frac{G}{\Delta}\int_0^{2\pi} dw' \int_0^{\infty} du' \frac{\Sigma(u',w')\left(\sinh^2 u' + \cos^2 w'\right)}{\{[\cosh(u-u') - \cos(w-w')]\,[\cosh(u+u') + \cos(w+w')]\}^{1/2}}. \qquad (5)$$

numerically and tabulate it on a grid in (u, w).

A choice for $\mu(a)$ that produces a disk with a central density minimum and a manageable outer cutoff is

$$\mu(a) = \mu_0(a-\Delta)\exp\left[-\frac{(a-a_0)^2}{2\sigma^2}\right], \qquad (6)$$

where the leading factor prevents density singularities at the foci. The numerical results below are computed in units where $G = M = \Delta = 1$. Taking $a_0 = 2$ places the peak density on orbits with eccentricities close to $e = 0.5$; for comparison, the innermost ringlet in the T95 model, which contributes most of the density in P1, has $e = 0.44$. I consider two models with $\mu(a)$ as given in equation (6) and $a_0 = 2$: a "wide" disk with $\sigma = 0.5$, and a "narrow" disk with $\sigma = 0.2$. The center of mass is at $x = -1.5$ for both disks. The surface densities are shown in figure 1, along with some representative orbits. I emphasize again that the purpose of these models is only to provide a plausible perturbing potential.

3. Periodic Orbits

Both the disk models discussed above and the T95 model are built entirely from aligned, periodic orbits. A real self-gravitating disk with finite velocity dispersion will be made predominantly from quasiperiodic orbits whose parents are nearly elliptical, periodic orbits elongated in the same

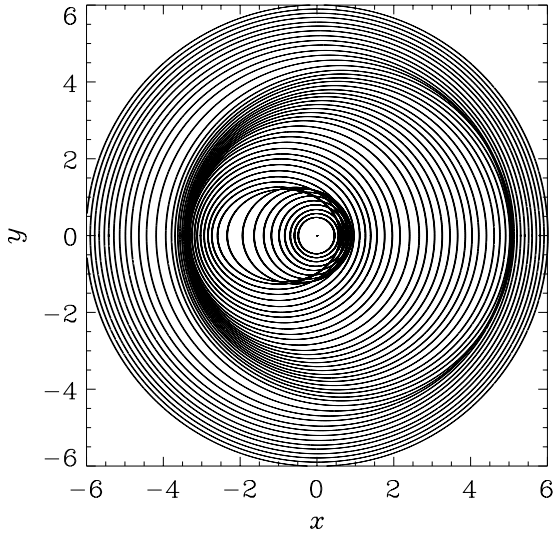

Fig. 2.— Closed periodic orbits in the wide disk, including self-gravity and uniform precession, for a disk mass $m = 0.025$ and precession speed $\Omega = 0.006$. The radial variation of eccentricity is required for uniform precession, and forces the crowding of orbits near the region of peak density.

sense as the disk. As long as the dispersion is not too large, the kinematics of the quasiperiodic orbits will approximately follow that of their periodic parents. Therefore a first approximation to the disk kinematics can be found by examining the sequence of periodic orbits elongated in the x direction in the perturbed potential. Consider the effect of the perturbation on purely Keplerian orbits. If it were fixed in an inertial frame, the perturbing potential [equation (5)] would initially drive a precession of each Kepler orbit at a frequency $\Omega(a, e)$, depending on semimajor axis and eccentricity. Alternatively, if it were fixed in a frame rotating at frequency $\Omega(a, e)$, then the perturbed orbit with that a and e would be closed in the rotating frame. I assume that the disk is stationary in a frame rotating at a fixed precession speed Ω_p; then the set of orbits satisfying $\Omega(a, e) = \Omega_p$ are the closed orbits in the disk.

I calculate sequences of periodic orbits for various assumed values of Ω_p by direct integration of the equations of motion in a frame rotating about the system barycenter. Orbits are launched perpendicularly from the x axis and the initial velocities adjusted iteratively so that the next x axis crossing occurs with $v_x = 0$. This procedure is not intended to find all of the periodic orbits, only the nearly elliptical ones elongated in the x direction.

A typical sequence of orbits in the wide ($\sigma = 0.5$) disk is shown in Figure 2. This sequence is computed for a disk mass $m = 0.025$ and precession speed $\Omega_p = 0.006$. All of the numerical results below are computed using the same disk mass; to leading order the results depend only on the ratio m/Ω_p and thus can be scaled to other masses. Notice that: (1) the innermost and outermost orbits are nearly circular; (2) a maximum eccentricity is reached by orbits whose apoapsides are slightly

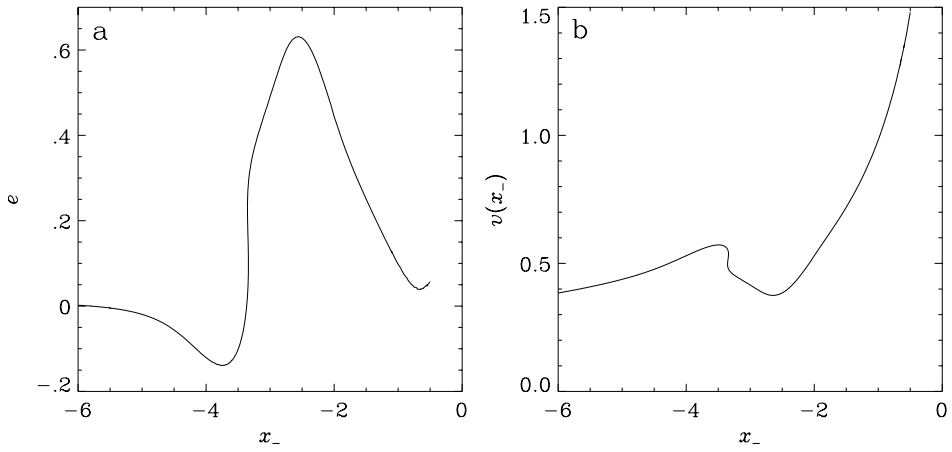

Fig. 3.— (*a*) Eccentricity of the orbits in Fig. 2 plotted against crossing point on the negative x axis. The eccentricity changes sign through the region of peak density, indicating that periapsis and apoapsis change sides with respect to the center. (*b*) Local orbital speed crossing the negative x axis plotted against x axis position. Velocities increase sharply outward just outside the density peak (at $x = -3.1$); the plotted function is actually double-valued owing to orbit crossing.

inside the peak density in the disk; and, most important, (3) many orbits of rapidly declining eccentricity pass through nearly the same apoapsis, in this case just outside the density peak.

Since the perturbed orbits are not precisely elliptical, eccentricity is defined here in terms of the points x_+ and x_- where the orbit intersects the positive and negative x axis, respectively. I let $e \equiv (x_- + x_+)/(x_- - x_+)$, so that $e > 0$ ($e < 0$) indicates periapsis at positive (negative) x. The run of e against x_- is shown in Figure 3a. Notice that e goes negative for orbits outside the density peak. It is easy to see why e has to change sign. Consider an orbit just inside the density peak. The perturbation can be approximated by an outward impulse applied to the orbit at apoapsis, which induces a precession in the prograde direction (Brouwer & Clemence 1961). Conversely, an orbit just outside the density peak receives an inward impulse, which must be applied at periapsis to cause precession in the same direction. The required gradient, $e' < 0$, is just what equation (1) says is needed to produce a mass concentration along the negative x axis. Note that equation (1) applies for e of either sign; thus in the region where $e < 0$, the outward increase in $|e|$ still contributes to the mass concentration at negative x. This argument also shows that the disk precession must be prograde, since retrograde precession would require $e' > 0$, putting the mass concentration on the wrong side to produce the needed impulse.[1] At smaller and larger a, $|e|$ returns to near zero. For these orbits, the perturbation approximates a constant force in the negative x and r directions, respectively. In either case, the precession rate contains a leading factor $(1 - e^2)^{1/2}/e$ (Brouwer

[1]Goldreich & Tremaine (1979) apply a similar argument the ϵ ring of Uranus. In that situation, however, the ring self-gravity acts to *lower* the precession rate driven by the Uranian quadrupole; hence the eccentricity increases outwards and the densest part of the ring is at periapsis.

& Clemence 1961). Orbits more distant from the density peak must therefore be less eccentric to maintain the same precession rate.

Relatively simple celestial mechanics thus shows that e must change sign (in the convention used here, from positive to negative) in any near-Keplerian disk with an eccentric density peak, in order for the disk to precess uniformly. The change in the sign of e means that stars contributing to the inner part of the density concentration are lingering near apoapsis, having risen from smaller radii, while stars making up the outer part are swinging through periapsis, having fallen from larger radii. This is the key to the observable kinematic signature.

4. Effect on the Rotation Curve

Figure 3b shows the velocities of orbits crossing the negative x axis as a function of the crossing point x_-. The velocity falls below the local circular speed for $x_- > -3.4$ because of the positive eccentricity, then abruptly rises as e drops through zero. The function $v(x_-)$ is actually double-valued because the orbits are mutually crossing near apoapsis in the region where e is changing rapidly (Fig. 2). Orbit crossing occurs for both of the disk density models considered here, though it is reduced somewhat by higher precession speeds. The rather rapidly precessing case shown in Figures 2 and 3 was chosen more for clarity than for realism. In reality, the precession speed will be set by self-consistency. A reasonable estimate for Ω_p can be obtained by requiring that the orbit through the density maximum of the original confocal model precess with the disk, retaining its original eccentricity. This gives slightly slower speeds of $\Omega_p = 0.004$ for the wide disk and $\Omega_p = 0.006$ for the narrow disk, for a mass of 0.025.

The double-valued nature of the rotation curve in Figure 3b will, of course, be washed out by projection effects. To approximate the observable signature, I project the disk velocity fields for a line of sight parallel to the y axis, adopting for the disk density that of the original confocal model. To compare with the FOC rotation curve, I let the distance from the origin to the density maximum in the model correspond to the P1-P2 separation of $0\farcs49$. In the T95 model, the disk has an inclination of 77°, at which the FOC slit width of $0\farcs063$ projects to a width of $0\farcs28$ in the disk plane. This corresponds to a band of width $\Delta y = 1.8$ about the x axis, over which I integrate the line of sight velocity. Since I completely ignore any contribution from the bulge, either to the light or to the rotation, the results should not be taken too literally, especially near the center.

Figure 4a shows the projected rotation curve for the wide disk with $m = 0.025$ and $\Omega_p = 0.004$. The dip and outer bump produced by the steep part of the ellipticity profile are preserved in projection. The near-Keplerian profile at small x_- is smoothed into an inner bump by the central hole in the density distribution and by the finite slit width. The combination of these effects produces a wiggle similar to that in the M31 rotation curve (fig. 4c); note that there is no comparable feature on the anti-P1 side of the center in either model or data. For the wide disk, the model wiggle is quite a bit too broad, a discrepancy remedied somewhat by narrowing the mass distribution.

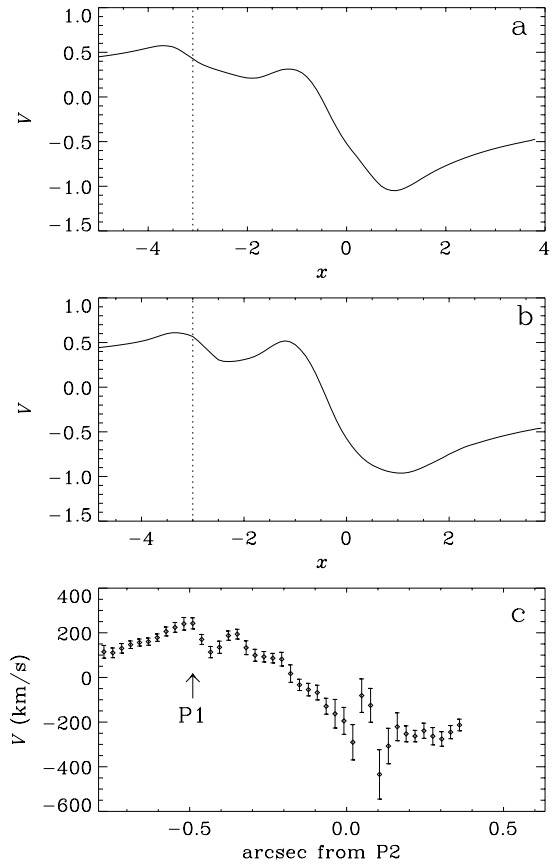

Fig. 4.— (*a*) Projected rotation curve for the wide disk, with mass $m = 0.025$ and precession speed $\Omega = 0.004$. Contributions from the bulge are ignored, and the velocity field is averaged over an aperture approximating the FOC slit (see § 4) laid along the disk major axis. Vertical dotted line marks the location of the peak density. (*b*) As in (*a*), but for the narrow disk with $m = 0.025$ and $\Omega = 0.006$. (*c*) Central region of the FOC rotation curve of M31, from Statler et al. (1999). Arrow marks the center of P1 and the location of the "P1 wiggle," the form of which is closely reproduced by the models.

Figure 4b shows the rotation curve for the narrow disk with the same mass and $\Omega_p = 0.006$. Though the fit is still not exact, the wiggle is noticeably narrowed; in particular, the outer bump now closely coincides with the density peak, in agreement with the FOC data. The results in Figure 4 are not qualitatively changed by $\pm 50\%$ variations in the assumed value of Ω_p.

5. Discussion

I have shown that in an eccentric near-Keplerian disk with an off-center density concentration, the disk's self-gravity will affect the periodic orbits in such a way as to produce an observable signature in the projected rotation curve. This signature is a "wiggle" extending through the

region of peak density, with a local velocity maximum at or just outside the peak, and a dip in the rotation curve just inside. Details interior to this region depend on the density structure, viewing geometry, and resolution. For a mass distribution resembling that of the T95 model for the M31 double nucleus, the computed wiggle closely resembles the observed FOC rotation curve through P1. This agreement gives strong support to the basic correctness of the eccentric disk picture.

A better understanding of the dynamics of M31's nuclear region should lead to more accurate mass determinations for the central BH. An enticing notion is that the P1 wiggle could be used to constrain the disk-to-BH mass ratio, and thereby the mass of the BH by way of an assumed mass-to-light ratio for the disk. Unfortunately, this is easier said than done. Disk models with the same value of m/Ω_p produce the same eccentricity law and rotation curve, to leading order. Constraining the mass would thus require an independent estimate of the precession speed. The T95 model has a disk mass of 0.16, which would imply $\Omega_p \sim 0.03$, by the arguments of § 4. Approximating the potential as Keplerian, this would put an inner Lindblad resonance (ILR) outside the dense part of the disk, in the vicinity of $r \sim 1''$. But whether one should expect to detect an ILR in a predominantly hot stellar system is, to say the least, problematical.

More realistic disk models will be needed both to obtain an accurate mass for the central BH and to understand the stellar dynamics of the nucleus. The simple models presented here neglect some important complications. The $e(a)$ profile in Figure 3a for the periodic orbits would imply a much more sharply peaked density structure than assumed in the confocal models in § 2. But equation (1) for the surface density is no longer valid when the orbits intersect, which would appear to be a necessary consequence of self-gravity. In reality, the radial width of the disk will be determined by the velocity dispersion. A self-consistent disk will mainly be composed of quasi-periodic orbits librating about the closed orbits considered here.[2] Sufficiently high dispersion could wash out the kinematic signature of the periodic orbits; self-consistent models will be required to determine at what dispersion this occurs. If the P1 wiggle is a sign of disk self-gravity, the challenge may really be to explain why M31's disk is dynamically cold enough for the effect to be visible.

This work was supported by NSF CAREER grant AST-9703036. The author is grateful to Ivan King, Joe Shields, Scott Tremaine, and Steve Vine for helpful comments.

[2]Examples of these loop-like orbits and their possible role in nuclear disks have recently been discussed by Sridhar & Touma (1999).

REFERENCES

Bacon, R., Emsellem, E., Monnet, G., & Nieto, J.-L. 1994, A&A, 281, 691

Brouwer, D. & Clemence, G. M. 1961, Methods of Celestial Mechanics (New York: Academic Press), Ch. 11.

Davoust, E. & Prugniel, P. 1990, A&A, 230, 67

Emsellem, E. & Combes, F. 1997, A&A, 323, 674

Gebhardt, K., Pryor, C., Williams, T. B., Hesser, J. E., & Stetson, P. B. 1997, AJ, 113, 1026

Goldreich, P. & Tremaine, S. 1979, AJ, 84, 1638

Kormendy, J., & Bender, R. 1999, ApJ, in press (KB99)

Lauer, T. R., Faber, S. M., Groth, E. J., Shaya, E. J., Campbell, B., Code, A., Currie, D. G., Baum, W. A., Ewald, S. P., Hester, J. J., Holtzman, J. A., Kristian, J., Light, R. M., & Westphal, J. A. 1993, AJ, 106, 1436

Lauer, T. R., Faber, S. M., Ajhar, E. A., Grillmair, C. J., & Scowen, P. A. 1998, AJ, 116, 2263

Sridhar, S. & Touma, J. 1999, MNRAS, 303, 483

Statler, T. S., King, I. R., Crane, P., & Jedrzejewski, R. I. 1999, AJ, 117, 894 (SKCJ)

Tremaine, S. 1995, AJ, 110, 628 (T95)